Life Cycle Assessment (LCA) of Worsted and Woollen processing in wool production: ReviWool® noils and other wool co-products

Composites Science and Technology 246 (2024) 110376

Contents lists available at ScienceDirect

Composites Science and Technology

journal homepage: www.elsevier.com/locate/compscitech

Fatigue life assessment of notched laminated composites: Experiments and modelling by Finite Fracture Mechanics

A.M. Mirzaei [a,*], A.H. Mirzaei [b], M.M. Shokrieh [b], A. Sapora [a], P. Cornetti [a]

[a] Department of Structural, Geotechnical and Building Engineering, Politecnico di Torino, Corso Duca degli Abruzzi 24, 10129, Torino, Italy
[b] Composites Research Laboratory, Center of Excellence in Experimental Solid Mechanics and Dynamics, School of Mechanical Engineering, Iran University of Science and Technology, Tehran, 16846-13114, Iran

ARTICLE INFO

Keywords:
Finite Fracture Mechanics
Fatigue life
Stress concentrations
Laminated composites
Theory of critical distances

ABSTRACT

In this paper, the coupled Finite Fracture Mechanics criterion is extended to assess the finite fatigue life of orthotropic notched laminated composites. The approach is validated through a comprehensive experimental program conducted on laminated composites under tension-tension cyclic loading conditions with two distinct lay-ups. For a given loading ratio, fatigue tests on plain and cracked specimens are first performed to provide the model inputs, the critical cyclic stress and stress intensity factor amplitudes. Fatigue tests on samples weakened by circular holes of two different radii are then used for blind predictions. Accurate predictions of the number of cycles to failure are achieved without the need for inverse calibration of material properties or deviation from standard testing procedures. Finally, a parametric study is performed to investigate the hole radius effect. It is worth mentioning that the proposed approach is general and can be applied to any notched geometry.

1. Introduction

Fiber-reinforced polymeric laminated composites have emerged as serious alternatives to traditional materials in various fields, due to their superior mechanical behavior and the ability to tailor their material characteristics [1–4]. However, the structural integrity of laminated composites is significantly influenced by the presence of geometric discontinuities, such as cracks or notches. Considering that notches are commonly encountered in engineering structures [5–7] and that fatigue is the most frequent failure mechanism [8], understanding the fatigue behavior of notched laminated composites is crucial for ensuring the reliability and safety of composite structures [9–12], particularly in aerospace, wind, and automotive engineering [13,14]. In recent decades, several criteria, initially proposed in the static framework, have been generalized to predict the fatigue failure of composite materials, encompassing either strain- [8], stress- [15], or energy-based [16] approaches.

Earlier investigations on the notch failure behavior of composite materials coupling linear elastic mechanics with a material length date back to the pioneering work by Whitney and Nuismer [17]. According to their approach, failure occurs when effective stress at or along a critical distance from the notch tip reaches its critical value, i.e., the ultimate strength. The critical distance was determined empirically (although a theoretical dependence on the fracture toughness was suggested) through a fitting procedure for predictions of the effect of both sharp notches and circular holes. The model was employed by several researchers to investigate the failure of notched components both in the static [2,18–23] and in the fatigue [24] loadings.

Whitney and Nuismer [17] introduced the fundamental concepts of the theory of critical distances (TCD), formalized almost thirty years later by Taylor [25]. The great merit of the work by Taylor [26] was to express the critical distance as a function of the material properties, through the (squared) ratio between the tensile strength and the fracture toughness. The distance being a material property, it represents a model input. Under monotonic loading, TCD has been successfully applied to estimate the notch effect in long-fiber composites [27] and short glass fiber reinforced polyamide 6 (SGFR-PA6) [28,29]. On the other hand, to the best knowledge of the present authors, the TCD approach has not been extended to estimate the fatigue lifetime of notched laminated composites yet. It should be noted that.

- The inherent flaw model by Waddoups et al. [30] gives predictions equivalent to TCD ones [26]. The criterion assumes that the strength of notched composites is governed by fracture instability, modelled

* Corresponding author.
E-mail address: amir.mirzaei@polito.it (A.M. Mirzaei).

https://doi.org/10.1016/j.compscitech.2023.110376
Received 27 September 2023; Received in revised form 12 November 2023; Accepted 30 November 2023
Available online 5 December 2023

through an ideal crack concept. The approach was employed to analyse the failure behavior of different material composites [31–33].

- In several works [20,34], it was noticed that optimal predictions can be achieved by increasing the critical distance with increased notch size. For this purpose, some empirical laws were introduced in related studies with more or less success.
- Since the TCD approach relies on the critical distance which is a material constant, it may not be suitable for small-size elements, where the critical distance exceeds the structural dimension.

To overcome the above limitations, Leguillon [35] and Cornetti et al. [36] introduced the Finite Fracture mechanics (FFM) approach. FFM considers a finite crack extension to be determined by coupling two distinct requirements, the stress, and energy condition. Thus, the crack advance becomes an output of the problem (and hence a *structural* property) and not an input (and a material property) as the critical distance is in the TCD approach. Under monotonic loading conditions, the approach has been successfully used for debonding analyses of composite structures [37,38], yielding results similar to those of the cohesive zone model - according to which the progressive degradation of material integrity at the interface is described through traction-separation laws - while reducing computational costs. Camanho et al. [39] employed the FFM approach to investigate the failure of open-hole laminated composites and demonstrated its capability to accurately predict experimental data. Then, FFM was employed to study the failure of laminated composites in different structural (geometrical/loading/material) configurations, e.g., mechanically fastened joints [40], irregular multi-bolt composite repairs [41], open holed laminates under mixed mode loading [42] and following an R-curve behavior [43]. Reinoso et al. [44] conducted a comparison between the results on notched thin-ply laminates obtained by the FFM and the phase field model - a widely used continuum-based approach in which failure from intact material to crack is characterized by a smooth function that delineates the evolution of damage - demonstrating the reliability and robustness of the FFM method.

The novelty of the present work is the extension and validation of the FFM approach for assessing the fatigue life of notched laminated composites. This task will be achieved experimentally, through an exhaustive test campaign on notched specimens, and semi-analytically, through the generalization of recent FFM studies on the fatigue behavior of (isotropic) metallic materials [45,46]. The paper is structured as follows. In Section 2, the stress field and the stress intensity factors of the tested geometries are provided. Then, in Section 3, the fundamentals of both TCD and FFM approaches are introduced, along with their extensions to cyclic loading. Section 4 presents the results of a comprehensive experimental campaign conducted on carbon/epoxy laminated composites with two different stacking sequences and four different geometries. In Section 5, a comparison between experimental data and theoretical predictions is provided and discussed, along with a parametric analysis of the effect of the hole radius. Finally, Section 6 is devoted to conclusions.

2. Linear elastic analysis of laminated composites

Let us consider orthotropic laminated composites of width W subjected to a cyclic uniaxial tensile remote stress with amplitude σ_a. The laminate is weakened either by a central circular hole of radius ρ (Fig. 1a) or by a crack of length $2a$ perpendicular to the loading direction (Fig. 1b).

In the current study, the failure mode of the composite laminate is assumed to be dominated by the fiber behavior, either brittle (i.e., fiber failure with minimal sub-critical damage) or characterized by fiber pull-out (with significant subcritical damage), see Refs. [5,47]. Hence, it is reasonable to assume that failure initiates and propagates along the x-axis, and mode I fracture will be investigated accordingly.

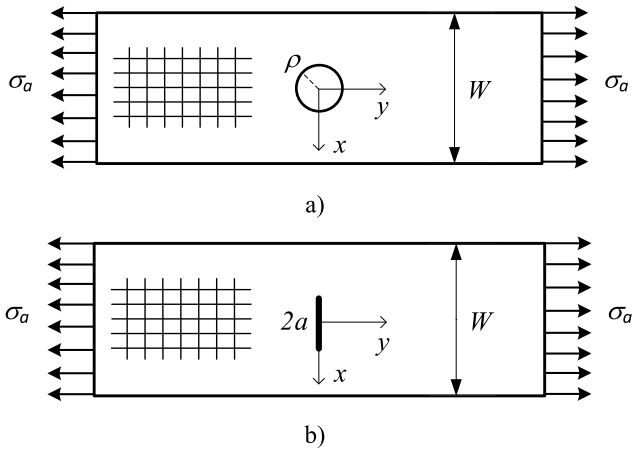

Fig. 1. Schematic view of a sample with (a) a circular hole, and (b) a crack under cycling remote uniaxial loading.

2.1. Stress field ahead of a circular hole

Konish and Whitney [48] presented an analytical solution to describe the distribution of normal stress perpendicular to the loading direction (i.e., for $y = 0$) ahead of a circular hole within an infinite orthotropic plate. The finite width of the specimens is taken into account by incorporating a correction factor, R_K, so that the stress field can be analytically approximated as ($x \geq \rho$):

$$\sigma_y(x) = \sigma_a \frac{R_k}{2}\left\{2+\left(\frac{\rho}{x}\right)^2+3\left(\frac{\rho}{x}\right)^4-\left(K_T^{\infty}-3\right)\left[5\left(\frac{\rho}{x}\right)^6-7\left(\frac{\rho}{x}\right)^8\right]\right\} = \sigma_a\, f_s(x) \tag{1}$$

where

$$K_T^{\infty} = \frac{\sigma_y(\rho)}{\sigma_a} = 1+\sqrt{\frac{2}{A_{22}}\left(\sqrt{A_{11}\,A_{22}}-A_{12}+\frac{A_{11}\,A_{22}-A_{12}^2}{2A_{66}}\right)} \tag{2}$$

$$R_K = \frac{K_T}{K_T^{\infty}} = \left\{\frac{3(1-2\,\rho/W)}{2+(1-2\,\rho/W)^3}+\frac{1}{2}\left(\frac{2\,\rho}{W}M\right)^6\left(K_T^{\infty}-3\right)\left[1-\left(\frac{2\,\rho}{W}M\right)^2\right]\right\}^{-1} \tag{3}$$

$$M = \sqrt{\frac{\sqrt{1-8\left[\frac{3(1-2\,\rho/W)}{2+(1-2\,\rho/W)^3}-1\right]}-1}{2(2\,\rho/W)^2}} \tag{4}$$

Note that K_T^{∞} and K_T represent the stress concentration factor at the opening edge of an infinite-width and a finite-width laminate, respectively. The components A_{ij} of the in-plane stiffness matrix of the laminate can be calculated based on the values provided in Table 2 (see Section 4.3).

2.2. Stress intensity factor for holed samples

Based on experimental observations [49], in a specimen like that depicted in Fig. 1a, failure initiates and propagates through two symmetric cracks each of length a along the x-axis [19,39–42,44]. Notably, as stated in Refs. [39,50], as well as in comparison with numerical analyses, the influence of the anisotropy on the stress intensity factor (SIF) is weak and can be disregarded for the present configuration.

More in particular, taking into account the finite width, the SIF can

be approximated as [51,52]:

$$K_I = \sigma_a\, F_h\, F_w \sqrt{\pi\, a} = \sigma_a\ \sqrt{a}\ f_k(a) \tag{5}$$

$$F_h = 1 + 0.358\frac{\rho}{a+\rho} + 1.425\left(\frac{\rho}{a+\rho}\right)^2 - 1.578\left(\frac{\rho}{a+\rho}\right)^3 + 2.156\left(\frac{\rho}{a+\rho}\right)^4 \tag{6}$$

$$F_w = \sqrt{\sec\left[\frac{\pi\,\rho}{W}\right]\sec\left[\frac{\pi\,(a+\rho)}{W}\right]} \tag{7}$$

Note that the accuracy of Eq. (5) was stated to be within 2% of the boundary-collocation results.

2.3. Stress intensity factor for cracked samples

Let us now consider the cracked geometry (Fig. 1b). Taking into account the orthotropy of the material (by $Y(\xi)$) and the finite width of the plate (by $F(a/W)$), the SIF for a center crack with length $2a$ can be expressed according to Ref. [53], as follows:

$$K_I = \sigma_a \sqrt{\pi\, a}\, Y(\xi)\, F(a\,/\,W) \tag{8}$$

$$Y(\xi) = 1 + 0.1(\xi - 1) - 0.016(\xi - 1)^2 + 0.002(\xi - 1)^3 \tag{9}$$

$$F(a\,/\,W) = \left[1 - 0.025(a/W)^2 + 0.06(a/W)^4\right]\sqrt{\sec\frac{\pi(a/W)}{2}} \tag{10}$$

where the dimensionless parameter ξ is defined in terms of the engineering elastic constants of the material [53,54].

$$\xi = \frac{(E_1\, E_2)^{1/2}}{2\, G_{12}} - (\nu_{12}\, \nu_{21})^{1/2} \tag{11}$$

It was mentioned that the error associated with the use of Eqs. 8–11 is under 5 %.

3. Failure criteria

This section provides an introduction to TCD and FFM failure criteria within the static framework, followed by a deeper discussion on their extension to assess the fatigue lifetime of notched structures.

3.1. Theory of critical distances

The TCD in its line method (i.e. averaged) formulation argues that failure occurs when the mean value of the normal stress along the critical distance $l_{LM} = (2/\pi) \times l_{ch}$ ahead the notch equals the ultimate strength X_t of the (quasi-brittle) material [17,25]; l_{ch} is Irwin's length, defined as $l_{ch} = (K_{Ic}/X_t)^2$, K_{Ic} being the material fracture toughness. In this context, the line method refers to the calculation of the mean value of the stress component over a line (path). Hence, referring to Fig. 1a, for example, the TCD model reads as follows:

$$\frac{1}{l_{LM}}\int_{\rho}^{\rho+l_{LM}} \sigma_y(x)\ \mathrm{d}x = X_t \tag{12}$$

3.1.1. Fatigue loading

In order to apply TCD in the static framework, input data of X_t and K_{Ic} are required. To extend the approach to finite life fatigue failure, the critical stress and SIF amplitude as a function of the number of cycles to failure, as stated in Ref. [55], are required. Wohler's curve for a plain (unnotched) specimen can be utilized as a representation of the variation of critical stress with the number of cycles to failure:

$$X_f = X_f(N) = a_x\ N^{-b_x} \tag{13}$$

Drawing inspiration from Basquin's equation [56], a power law variation on N can also be assumed for the critical SIF K_{If} [57,58]:

$$K_{If} = K_{If}(N) = a_k\ N^{-b_k} \tag{14}$$

Note that Eq. (14) is equivalent to employing a critical distance $l_{f,\,LM}$ that is dependent on the number of cycles to failure, based on a power-law equation. Eq. (15) shows that the parameters a_l and b_l are trivially dependent on a_x, b_x, a_k and b_k:

$$l_{f,LM} = l_{f,LM}(N) = \frac{2}{\pi}\left(\frac{K_{If}}{X_f}\right)^2 = a_l\ N^{-b_l} \tag{15}$$

In fact, in the original paper [55], the Authors directly used Eq. (15) instead of Eq. (14) obtaining the function $l_{f,LM}\ (N)$ using an inverse calibration method through stress-life data associated with the sharpest notched sample.

Now, by replacing X_t and l_{LM} in Eq. (12) with X_f and $l_{f,\,LM}$, we get:

$$\frac{1}{l_{f,LM}}\int_{\rho}^{\rho+l_{f,LM}} \sigma_y(x)\ \mathrm{d}x = X_f \tag{16}$$

Considering, for instance, the holed samples (Fig. 1a), using Eqs. (1), (13) and (15), Eq. (16) can be reformulated as:

$$\sigma_a \int_{\rho}^{\rho+a_l N^{-b_l}} f_s(x)\mathrm{d}x = a_x\ a_l\ N^{-(b_x+b_l)} \tag{17}$$

which, for a given nominal stress amplitude σ_a, represents an equation with a single unknown variable N and whose solution provides the number of cycles to failure, N_f.

The calibration of the two free parameters in $l_{f,\,LM}$ (Eq. (15)), a_l and b_l (or, equivalently, a_k and b_k for K_{If}), requires (at least) two data points. In the study presented in Ref. [55], two different approaches were proposed. The former involved utilizing two extreme cases in the finite fatigue life regime, namely the static and fatigue limits. The latter employed stress-life (SN) data from a notched specimen across a wide range of nominal stress amplitude to calibrate the critical distance. In the following this second method will be implemented, since it provides higher accuracy in the calibration process.

3.2. Finite Fracture Mechanics

In the static framework, the FFM failure criterion relies on a discrete crack extension denoted as l, which, differently from TCD, is determined along with the failure load by the simultaneous fulfillment of a stress requirement and the finite energy balance [35,36]. The former (stress) requirement is analogous to the one used by the TCD. The latter condition ensures sufficient energy for finite crack growth and can be written in terms of the SIF, exploiting Irwin's relationship. For instance, for the holed geometry (Fig. 1a), the FFM criterion (in its averaged formulation) reads as follows:

$$\begin{cases} \dfrac{1}{l}\displaystyle\int_{\rho}^{\rho+l} \sigma_y(x)\ \mathrm{d}x \geq X_t \\ \dfrac{1}{l}\displaystyle\int_{0}^{l} K_I^2(a)\ \mathrm{d}a \geq K_{Ic}^2 \end{cases} \tag{18}$$

While FFM appears as a system of two inequalities, it is easy to verify that the minimum load at which both inequalities are satisfied occurs when they are strictly fulfilled [36]. In other words, for the so-called positive geometries (i.e., the most common case), the inequality system in Eq. (18) reverts to a system of two equations in two unknowns: the failure load (e.g., the critical remote stress, which is embedded in both the stress field and the SIF) and the critical (finite) crack advance.

It is worth noting that FFM treats the critical distance (i.e., the discrete crack extension) as an output rather than an input. This implies that it depends not only on the material properties but also on the geometry of the structure. Note also that FFM does not require any additional material property compared to the TCD approach. Finally, FFM

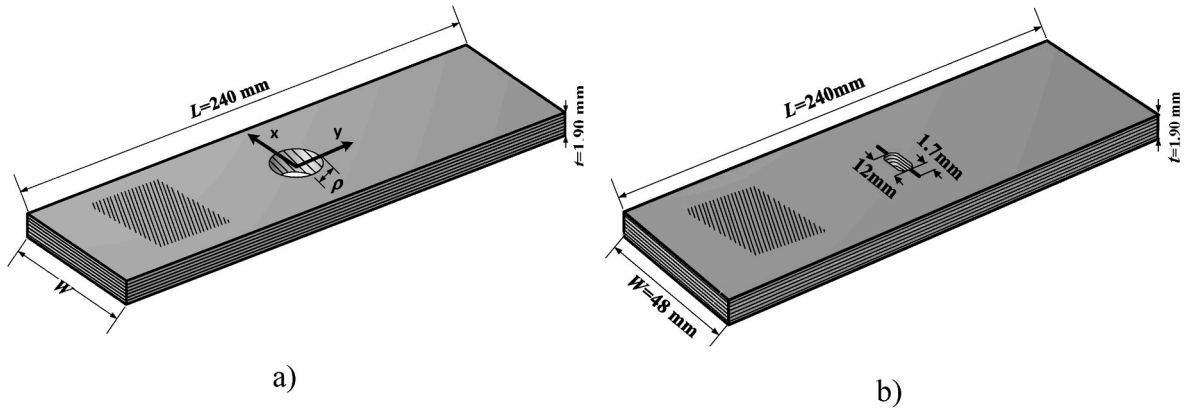

Fig. 2. Schematic view of the fabricated notched specimens. (a) Holed ($W = 24$, 36 mm and $\rho = 2.1$, 3.25 mm) and (b) cracked geometry.

can be seen as an improvement of the TCD approach, since the stress-energy coupling allows for the consideration of the material-geometry interaction, while usually TCD becomes unreliable when the structural size approaches the critical distance.

3.2.1. Fatigue loading

The extension of the FFM criterion to estimate the finite fatigue life of notched components was recently proposed by Mirzaei et al. [45] and it consists of replacing X_t and K_{Ic} in Eq. (18) with the functions $X_t(N)$ – Eq. (13) – and $K_{If}(N)$ – Eq. (14). In this way, for a given nominal stress amplitude σ_a, the system presented in Eq. (17) becomes a system of two inequalities with two unknowns, the number of cycles to failure, N_f – the minimum among all the admissible values – and the corresponding finite crack extension, l_f. By making explicit N from both the inequalities, Eq. (18) yields:

$$\begin{cases} N \geq \left(\dfrac{a_x \; l}{\sigma_a \; \int_\rho^{\rho+l} f_s(x)\, \mathrm{d}x} \right)^{\frac{1}{b_x}} \\ N \geq \left(\dfrac{a_k^2 \; l}{\sigma_a^2 \; \int_0^l a \; f_k^2(a)\, \mathrm{d}a} \right)^{\frac{1}{2b_k}} \end{cases} \tag{19}$$

For a given stress amplitude σ_a and radius ρ, the first equation implies an increasing N as l increases (since the stress is usually monotonically decreasing moving away from the notch), while the second one implies a decreasing N as l grows (since, for positive geometries, the SIF increases with the crack length), see also Section 5. Thus, it is clear that the minimum N for which both inequalities are fulfilled is at the intersection point between the two curves: the ordinate of such a point is the number of cycles to failure N_f, i.e., the main unknown of the fatigue problem, whereas the abscissa defines the critical crack extension l_f. Analytically, N_f has to be determined by solving the equation obtained by equating the two right-hand sides in the system of Eq. (19):

$$a_x^{2b_k} (l/\sigma_a)^{2(b_k - b_x)} \left(\int_0^l a \; f_k^2(a)\, \mathrm{d}a \right)^{b_x} = a_K^{2b_x} \left(\int_\rho^{\rho+l} f_s(x)\, \mathrm{d}x \right)^{2b_K} \tag{20}$$

For a given stress amplitude σ_a and radius ρ, Eq. (20) represents an implicit equation in the finite crack advance l_f. Its substitution into either the first or the second equation of the system of Eq. (19) yields the number of cycles to failure N_f.

Finally, two remarks about the comparison between TCD and FFM approaches are outlined.

1. The critical crack advance according to FFM is generally not a power law function of the number of cycles to failure, as supposed in the TCD model (Eq. (15));
2. In the static framework, TCD (Eq. (12)) does not require equation solving, making it more advantageous from a computational point of view. However, in the fatigue context, both TCD and FFM approaches require the (numerical) solution of an equation (Eq. (17) or Eq. (20), respectively) and, hence, are equivalent in terms of computational costs.

4. Experimental campaign

To validate the approach presented in the previous section, an experimental campaign was conducted on laminated composites. Two laminates with different stacking sequences were considered. In addition to static tests aimed at determining the elastic parameters, fatigue tests were performed on plain, cracked, and notched geometries. The latter were machined using drilled circular holes of two different radii.

4.1. Materials and fabrication of samples

The specimens utilized in the experimental campaign were composed of carbon fiber (T300-12K, 200 g/m^2) and a low viscosity epoxy resin (Araldite LY 5052) cured with Aradur 5052 Hardener in a

Table 1
Specifications of the performed experimental tests.

	Specimen configuration	Layup	W (mm)	L (mm)	t (mm)	Aim	Type of loading	Number of tests
1	Longitudinal loading	$[0_6]_t$	15	250	1.44	Material characterization	Static loading	4
2	Transverse loading	$[90_{10}]_t$	25	175	2.2	Material characterization	Static loading	4
3	Shear loading	$[45/\text{-}45]_{4s}$	25	200	3.53	Material characterization	Static loading	4
4	Cross-ply, plain	$[0/90]_{2s}$	25	240	1.9	Model characterization	Fatigue loading	10
5	Cross-ply, cracked $a = 15.4$ mm	$[0/90]_{2s}$	48	240	1.9	Model characterization	Fatigue loading	8
6	Cross-ply, drilled $\rho = 2.1$ mm	$[0/90]_{2s}$	24	240	1.9	Model validation	Fatigue loading	8
7	Cross-ply, drilled $\rho = 3.25$ mm	$[0/90]_{2s}$	36	240	1.9	Model validation	Fatigue loading	7
8	Cross-ply, plain	$[90/0]_{2s}$	25	240	1.9	Model characterization	Fatigue loading	9
9	Cross-ply, cracked $a = 15.4$ mm	$[90/0]_{2s}$	48	240	1.9	Model characterization	Fatigue loading	7
10	Cross-ply, drilled $\rho = 2.1$ mm	$[90/0]_{2s}$	24	240	1.9	Model validation	Fatigue loading	8
11	Cross-ply, drilled $\rho = 3.25$ mm	$[90/0]_{2s}$	36	240	1.9	Model validation	Fatigue loading	11

Table 2
Material properties of T300/LY5052 unidirectional composites.

Property	Symbol	Magnitude
Longitudinal modulus	E_1	102 GPa
Transverse modulus	E_2	8.5 GPa
In-plane shear modulus	G_{12}	6 GPa
Poisson's ratio	ν_{12}	0.31
Ultimate tensile strength	X_t	914 MPa
Transverse strength	Y_t	21 MPa
In-plane shear strength	S_{xy}	78 MPa
Ply thickness	t	0.235 mm
Fiber volume fraction	ν_f	54 %

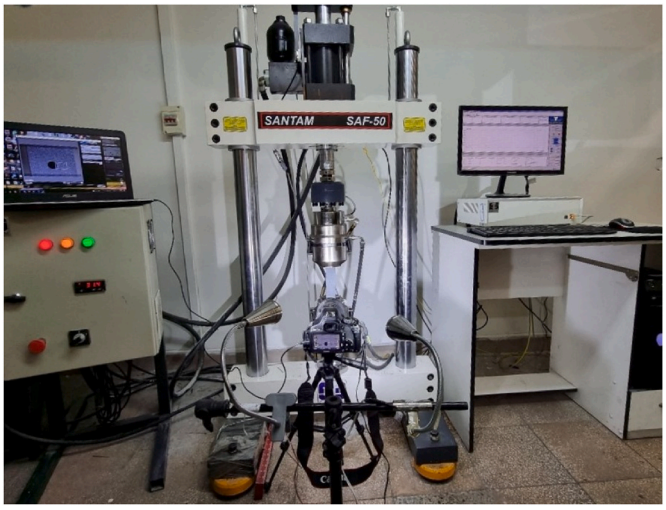

Fig. 3. Experimental setup used to conduct the experimental tests.

weight fraction of 100:38, employing the vacuum-assisted resin injection method. Following the instructions provided by the supplier, the laminated composites were cured at 23 °C for one day and subsequently post-cured at 100 °C for 4 h.

The samples were obtained by cutting a laminated composite plate using a waterjet machine. To create the holed samples, the central holes were drilled to their final size using a drill press operating at a relatively slow speed of 300 RPM. This approach was chosen to avoid severe delamination at the hole circumference, which is commonly observed when using the waterjet machine, especially for small diameters. To introduce cracks into the specimens, a 12 mm slit with a width of 2 mm was created at the center of each sample using waterjet cutting. Subsequently, cracks with a length of 1.7 mm were carefully formed on both sides of the slit (i.e. pre-crack) using a thin razor blade, resulting in a total crack length of $a = 15.4$ mm [59]. Afterward, all the lateral surfaces of the specimens, as well as the hole surfaces, were smoothed using sandpaper. Finally, specimens were equipped with a quasi-isotropic layup of glass/epoxy tabs with $[0/90/45/\text{-}45]_s$ configuration. Fig. 2 provides a schematic view of the fabricated notched specimens in the present study. Also, Table 1 presents the geometrical properties of the fabricated specimens with/without stress concentration for the characterization and evaluation of the proposed models. It is noteworthy that the ratio of width to hole radius for the drilled specimens remained approximately constant at 6.

4.2. Testing setup and experimental details

Both static and fatigue tests were carried out using the Santam SAF-50 machine equipped with hydraulic grips, in the School of Mechanical Engineering of Iran University of Science and Engineering. To prevent self-heating and temperature rise in the specimens during fatigue tests, a frequency of 5 Hz was applied [11,60,61]. Furthermore, to minimize the influence of out-of-plane stresses, the experimental variables were designed to minimize the probability of delamination in the laminated

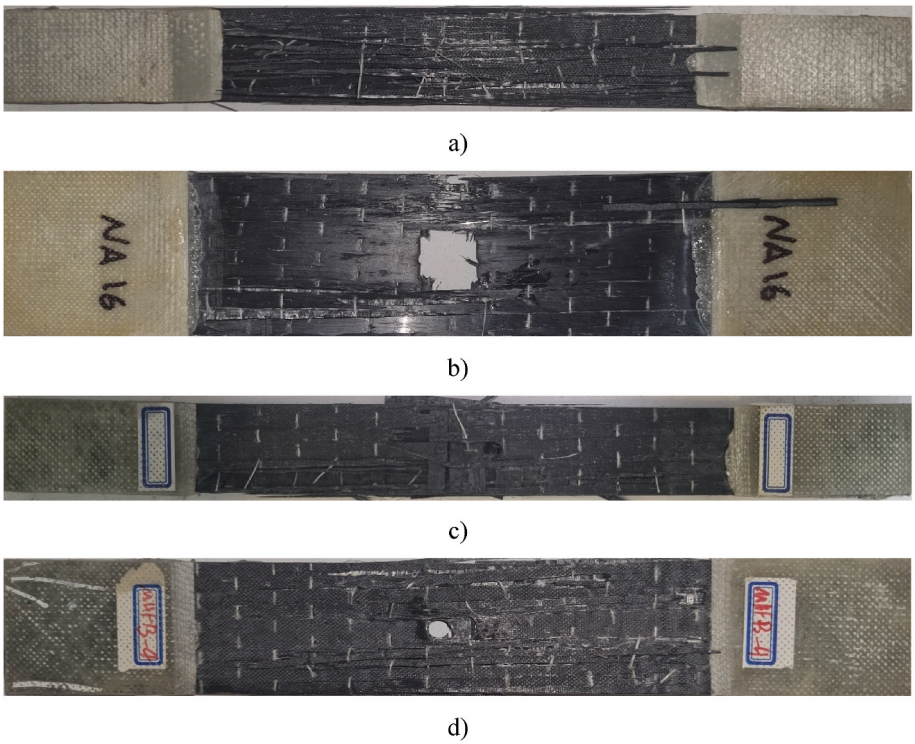

Fig. 4. Specimens after fatigue failure in a fiber pull-out failure mode: (a) plain, (b) cracked (c) holed with $\rho = 2.1$ mm and (d) holed with $\rho = 3.25$ mm.

composites. This was achieved by setting the stress ratio (minimum stress/maximum stress) to 0.1 and using low-thickness specimens [62]. The experimental setup employed for the testing is illustrated in Fig. 3.

It is worthwhile to note that the notch sensitivity of a laminate depends on various factors including size, thickness, ply orientation, notch geometry, and material constituents [63]. Studies conducted by Harris and Morris [64] and Vaidya et al. [65] examined the impact of increased laminate thickness on strength and found that increased thickness led to damage confinement near the surface and altered the failure mechanism to delamination. Therefore, it is crucial to ensure that the failure mode of samples is either brittle or fiber pull-out for proper application of the models in laminated composites.

4.3. Static tests, material characterization

The ASTM D3039 standard [66] was employed to determine the longitudinal and transverse mechanical properties (i.e., elastic moduli, ultimate tensile strength, and Poisson's ratio), and in-plane shear properties were obtained using the ASTM D3518 standard [67]. Table 2 presents the results of the quasi-static tests (average of four tests), which were conducted to determine the material properties. It is worthwhile to mention that the fiber-to-matrix volume fraction was obtained using the burn-out method outlined in the ASTM D3171 standard [68].

Considering [63], the ply thickness of the material is relatively high, measuring $t = 0.235$ mm. Thus, as depicted in Fig. 4, the predominant failure mode observed was primarily attributed to the fiber pull-out effect, with no specimens failing due to brittle failure. It is worthwhile to emphasize that this figure shows the specimens after failure, which may affect the visual interpretation of initial features.

4.4. Fatigue tests

The stress-life (SN) diagrams for $[90/0]_{2s}$ and $[0/90]_{2s}$ layups are depicted in Figs. 5 and 6, respectively. These diagrams present the experimental data obtained by testing both plain and cracked specimens (used for characterization), as well as specimens weakened by holes with radii $\rho = 2.10$ and 3.25 mm. According to Table 1, a total number of 33 for $[0/90]_{2s}$ and 35 samples for $[90/0]_{2s}$ were tested, with 7–11 samples considered for each notch geometry. The diagrams are presented in a log-log format, with the nominal (gross-section) stress amplitude, σ_a, plotted against the number of cycles to failure, N_f, defined as the complete detachment of the specimens. The fatigue loading amplitudes were randomly selected for each test to evaluate the material response under a variety of stress levels. The solid black lines represent the best-fitting curves based on the experimental data (probability of survival, PS, 50 %). The scatter bands, indicated by dashed red lines, represent a PS of 97.7 % and 2.3 %.

To compare fatigue test results, the best-fitting curves for all the studied cases were plotted in Fig. 7. This figure provides a clear perspective on the fatigue behavior of laminated composites, considering cases with or without stress concentrators, under various loading levels. By analyzing the trends, valuable insights can be gained regarding the performance of the laminated composites in different scenarios.

1. The $[90/0]_{2s}$ layup demonstrates higher fatigue strength compared to the $[0/90]_{2s}$ layup. This can be attributed to the mechanical interaction between the 0° and 90° fibers. In the laminated composites, the 0° fibers are primarily responsible for carrying the load, while the 90° fibers provide crucial lateral supports for the 0° fibers. For the $[90/0]_{2s}$ layup, the outermost 0° layers are backed by 90°

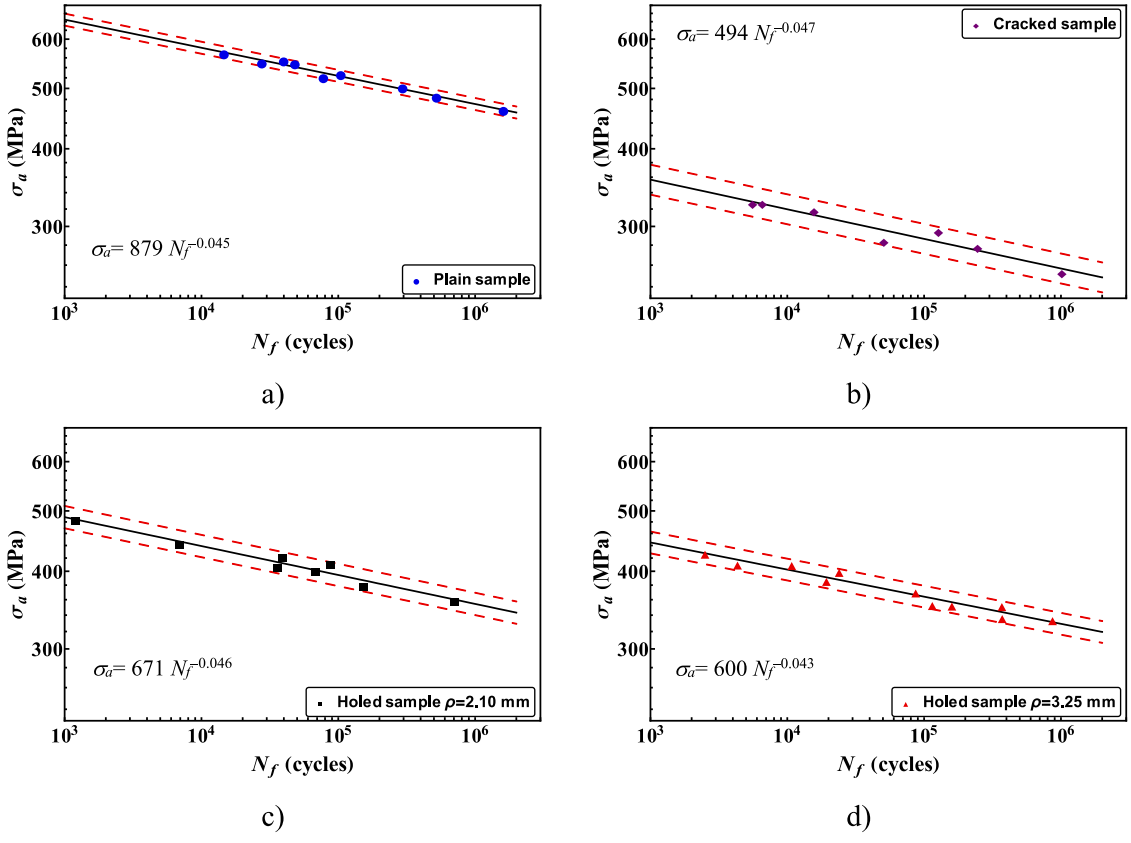

Fig. 5. Stress-life diagrams for $[90/0]_{2s}$ laminated composites: (a) plain sample, (b) cracked sample, (c) samples weakened by a hole with radius $\rho = 2.1$ mm, and (d) $\rho = 3.25$ mm. The dashed red lines represent a PS of 97.7% and 2.3%.

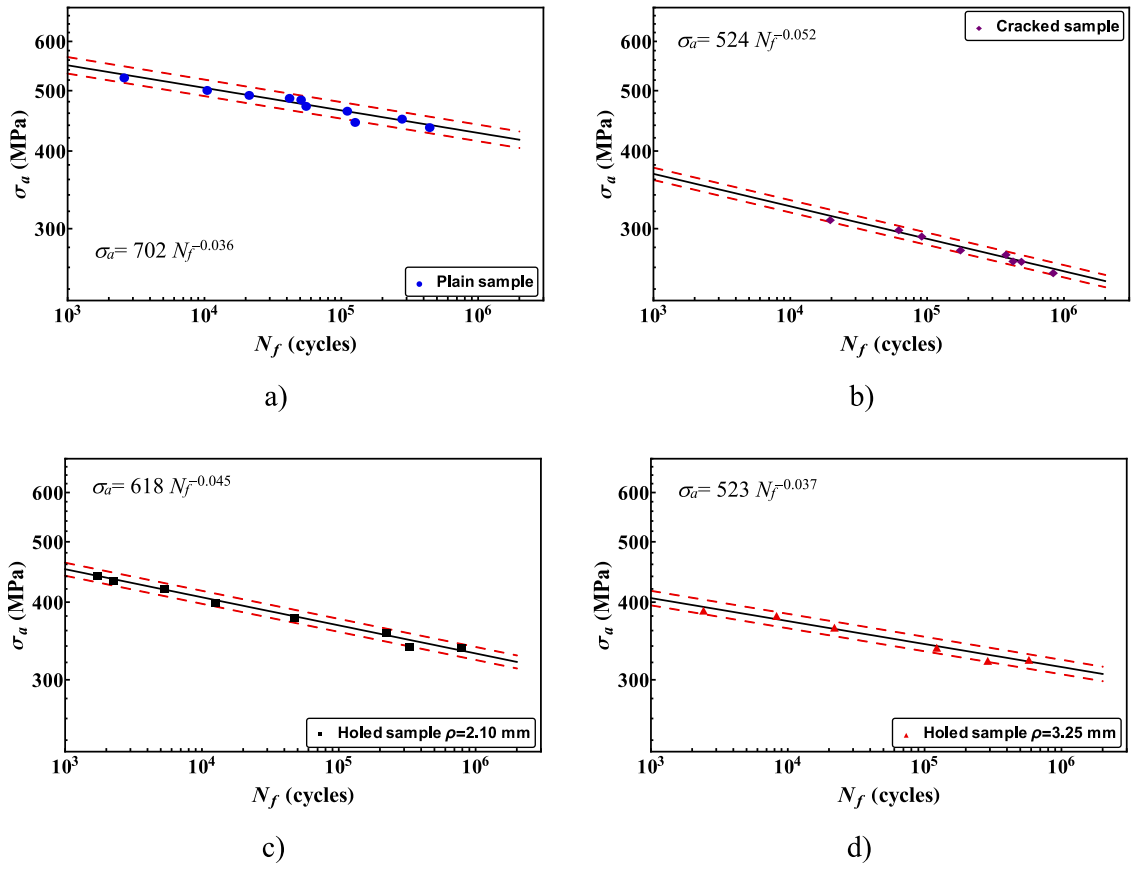

Fig. 6. Stress-life diagrams for $[0/90]_{2s}$ laminated composites: (a) plain sample, (b) cracked sample, (c) sample weakened by a hole with radius $\rho = 2.1$ mm, and (d) $\rho = 3.25$ mm. The dashed red lines represent a PS of 97.7 % and 2.3 %.

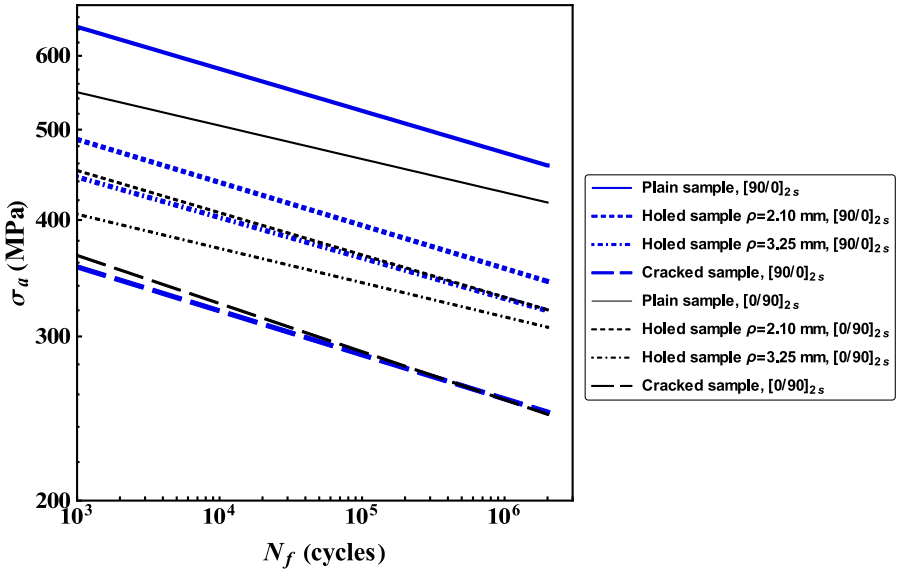

Fig. 7. Stress-life diagrams for all investigated laminated composites – power-law best-fitting curves for the eight experimental data sets.

layers. This configuration might result in a more effective transfer of load and a higher resistance to failure.

2. As the stress concentration/singularity increases (from plain to crack), the critical stress amplitude decreases for the same number of cycles to failure. Moreover, the differences in critical stress amplitude between the two layups are reduced.
3. For holed specimens, it is observed that their strength decreases - with a fixed number of cycles - as the radius of the hole increases. This trend mirrors the conventional size effect exhibited in isotropic materials [39], confirming that the predominant cause of failure in these samples is fiber pull-out, not delamination.

Table 3
The calculated values of a_s, b_s, a_k, and b_k for both layups.

Layup	Eq. (13): $X_f(N) = a_x\ N^{-b_x}$ [MPa]	Eq. (14): $K_{If}(N) = a_k\ N^{-b_k}$ [MPa $\sqrt{m}$]
$[90/0]_{2s}$	$a_x = 879$ [MPa]	$a_k = 98$ [MPa$\sqrt{m}$]
	$b_x = 0.045$	$b_k = 0.047$
$[0/90]_{2s}$	$a_x = 702$ [MPa]	$a_k = 107$ [MPa$\sqrt{m}$]
	$b_x = 0.036$	$b_k = 0.052$

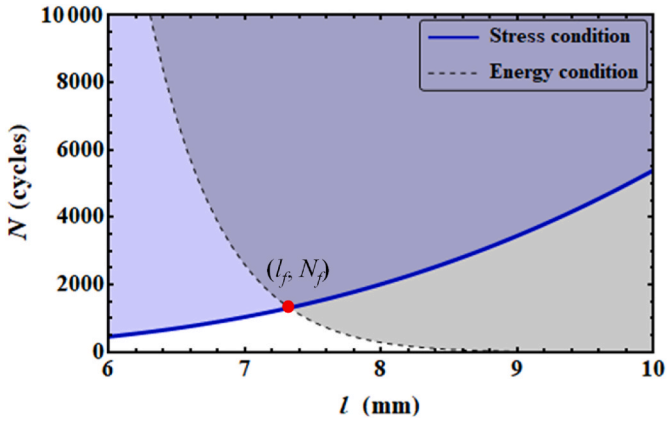

Fig. 8. A graphical representation of the FFM system for an arbitrary case of σ_a = 420 MPa, ρ = 2.1 mm and $[0/90]_{2s}$ layup.

5. Results and discussion

In this section, fatigue test data related to plain and cracked geometries are utilized to characterize the model, i.e., to obtain the two functions $X_f(N)$ and $K_{If}(N)$ (model characterization, see Table 1). Subsequently, blind predictions by TCD and FFM approaches are made for the two geometries with circular holes. A parametric analysis of the effect of the hole radius is also presented.

5.1. Model characterization and validation

As previously discussed in Section 2, the inputs for the models are functions $X_f(N)$ and $K_{If}(N)$. The best-fitting procedure employed for stress-life data of plain specimens (Fig. 5a and 6a) yielded values of a_x and b_x in Eq. (13), as reported in Table 3 for each stacking sequence. Analogously, stress (SIF)-life data of cracked specimens (Fig. 5b and 6b) resulted in obtaining a_k and b_k values (Eq. (14), Table 3).

With $X_f(N)$ and $K_{If}(N)$ available, blind predictions can be made for the fatigue data of holed samples. In the case of the TCD approach, Eq. (17) needs to be solved, while for FFM, the equation to be solved is Eq. (20). However, before proceeding, it is advisable to have a better understanding of the FFM system. For the sake of clarity, a graphical representation of the FFM system (Eq. (19)) is presented in Fig. 8 for an arbitrary case with σ_a = 420 MPa, ρ = 2.1 mm and $[0/90]_{2s}$ layup. Fig. 8 illustrates that stress and energy requirements vary monotonically with the finite crack advance l_f, resulting in l_f = 7.32 mm. Additionally, the predicted number of cycles to failure is the minimum value for which both inequalities are satisfied, with N_f = 1309 cycles.

For further study of the performances of both models, in Fig. 9, the critical distance/finite crack advance vs. N_f, predicted by TCD and FFM for both $[0/90]_{2s}$ and $[90/0]_{2s}$ stacking sequences are plotted. In the figure, the solid line represents the critical distance (calculated using Eq. (15)). The finite crack advance is determined by solving the system of equation (19), and the triangular data points correspond to the results obtained for a ρ = 2.1 mm, while the circular data points are associated with ρ = 3.25 mm.

The figure demonstrates that the finite crack advance, as determined by FFM, is influenced not only by material properties but also by geometric characteristics. In this case, a decrease in notch radius results in a reduced finite crack advance, consistently remaining lower than the TCD critical distance. Furthermore, for a constant N_f, the critical distance/finite crack advance for the $[0/90]_{2s}$ layup is higher than that of the $[90/0]_{2s}$ layup, with a more significant variation in the number of cycles. Thus, it can be concluded that the damage zone for $[0/90]_{2s}$ is larger than that for $[90/0]_{2s}$, resulting in the increased strength of the $[90/0]_{2s}$ layup, as already observed (Fig. 7).

An interesting observation is related to the $[90/0]_{2s}$ layup for the sample with a notch radius of 2.1 mm. In this case, the critical distance exceeds the sample ligament. To address this issue within the TCD

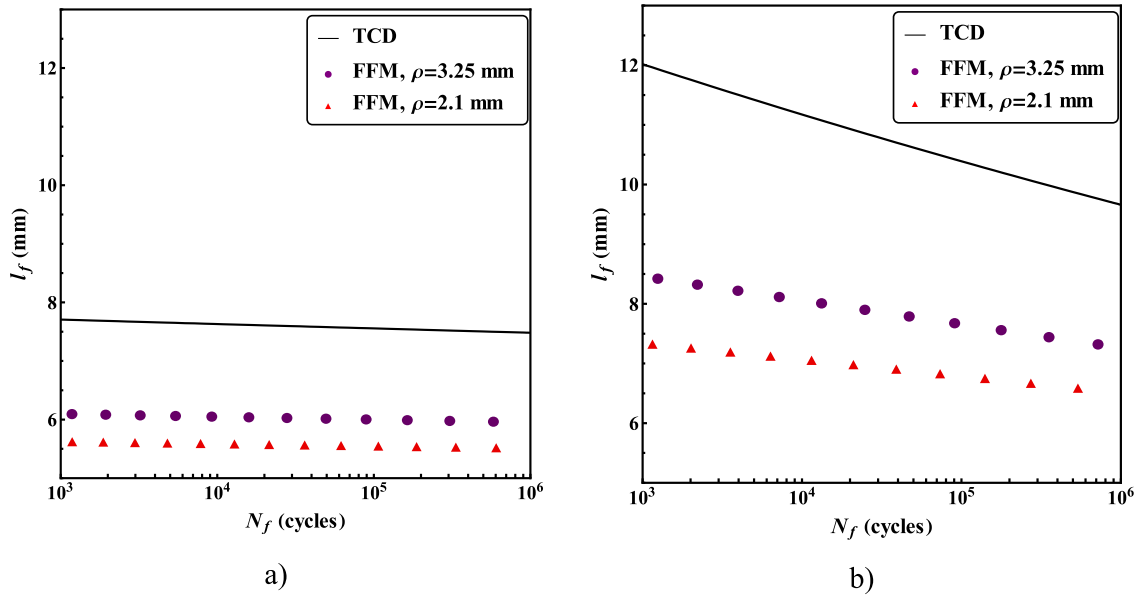

Fig. 9. The critical distance/finite crack advance vs. N_f for (a) $[90/0]_{2s}$, and (b) $[0/90]_{2s}$ layups in a linear-log plot. The solid line indicates the critical distance, and the triangular markers show the results for ρ = 2.1 mm, whereas the circular data points are related to ρ = 3.25 mm.

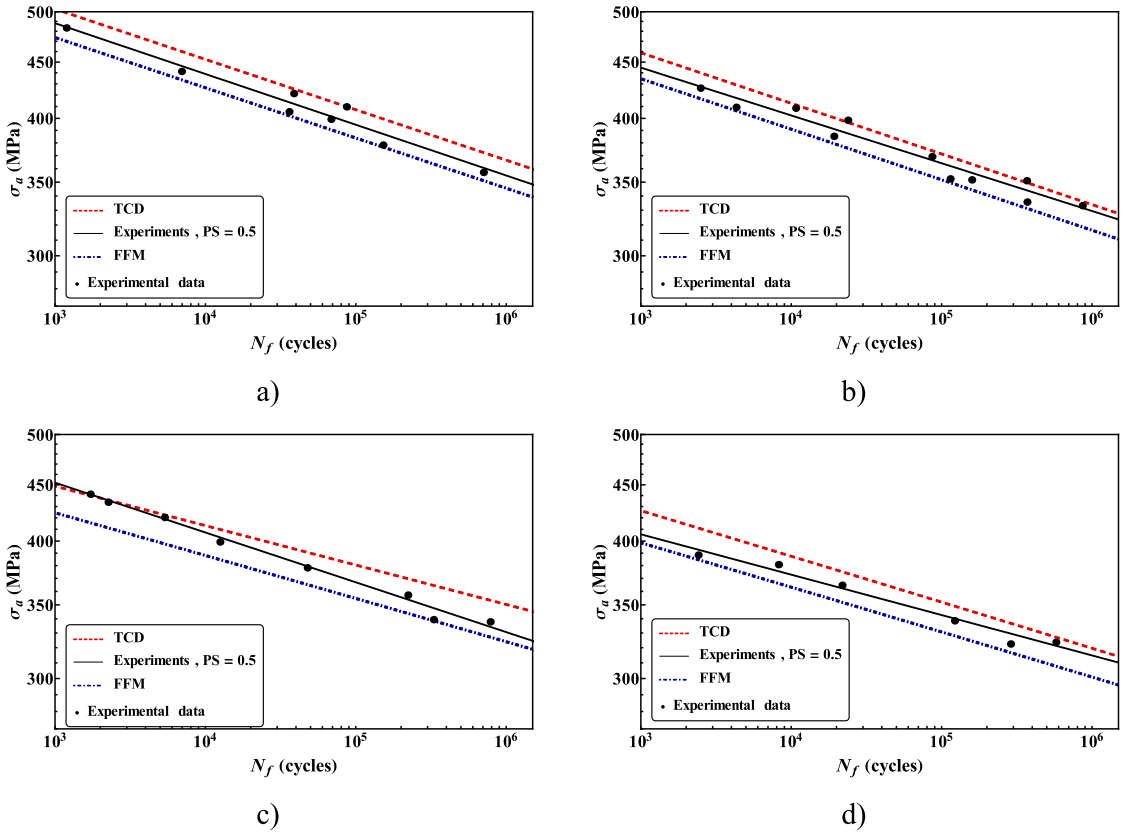

Fig. 10. Stress-life diagrams illustrating experimental data, along with predictions by TCD and FFM, for (a) $[90/0]_{2s}$ layup and $\rho = 2.1$ mm, (b) $[90/0]_{2s}$ layup and $\rho = 3.25$ mm, (c) $[0/90]_{2s}$ layup and $\rho = 2.1$ mm, (d) $[0/90]_{2s}$ layup and $\rho = 3.25$ mm.

approach, for this sample, a fixed critical distance of 10.4 mm was considered, presuming that this distance covers the entire ligament. However, it should be noted that this assumption could potentially affect the efficiency of the TCD approach in predicting fatigue lifetime. This drawback is not observed within the FFM approach.

For a comprehensive side-by-side comparison, the stress-finite fatigue life diagrams predicted by both models and corroborated by experimental data for each notched geometry and stacking sequence are illustrated in Fig. 10.

From this figure, it is evident that both approaches provide fatigue life predictions that closely align with the median fit line (PS equal to 0.5) of the experimental data. FFM results are consistently positioned below the median fit line across all four cases under consideration, thus always revealing conservative estimates. In contrast, TCD predictions are (almost) invariably higher than the median fit line, resulting in unconservative predictions. It is worthwhile to emphasize that in Fig. 10c (for the case with $[0/90]_{2s}$ layup and $\rho = 2.1$ mm), a fixed critical distance equal to 10.4 mm was assumed, coherently with what was discussed before.

Figs. 11 and 12 present the theoretical vs. experimental comparison in a different format, i.e., in terms of the estimated fatigue life N_f vs. the experimental one $N_{f,exp}$. Fig. 11 presents the results obtained by TCD, while Fig. 12 illustrates the results obtained by FFM. In both figures, the solid black line (inclined at 45°) indicates exact estimations, while the area above it refers to conservative predictions. The dashed blue lines correspond to the 1/3 and 3 scatter bands, and the dotted-dashed gray lines correspond to the 1/5 and 5 scatter bands.

Both TCD and FFM models exhibit strong potential in predicting the fatigue life of laminated composites. *R*-squared scores, which are correlation coefficients derived from the natural logarithm transformation of the data, fall impressively within a range of 0.81–0.86, highlighting the efficacy of these models. Upon comparison, the TCD model exhibits higher accuracy than the FFM model when compared to the experimental data. However, FFM results are always slightly conservative, which is advantageous for design purposes, while the TCD model tends to be unconservative.

5.2. *Parametric study on radius effect in holed samples*

A parametric study is finally conducted to investigate the effect of hole radius on the lifetime of both $[90/0]_{2s}$, and $[0/90]_{2s}$ layups. Only the results by the FFM model, which provides conservative results, are presented, generalizing to cycling loadings what was done in a static framework by Camanho et al. [39]. To mitigate numerical errors and avoid possible physical issues related to finite width, we fixed the width of all specimens to $W = 100$ mm, significantly larger than the maximum hole radius. Fig. 13a depicts the relationship between hole radii and the nominal (gross-section) stress amplitude, σ_a, for fixed lifetimes N_f, whereas Fig. 13b presents the effect of hole radius on the lifetime for fixed stress amplitudes σ_a. Note that the stress amplitudes in Fig. 13b are

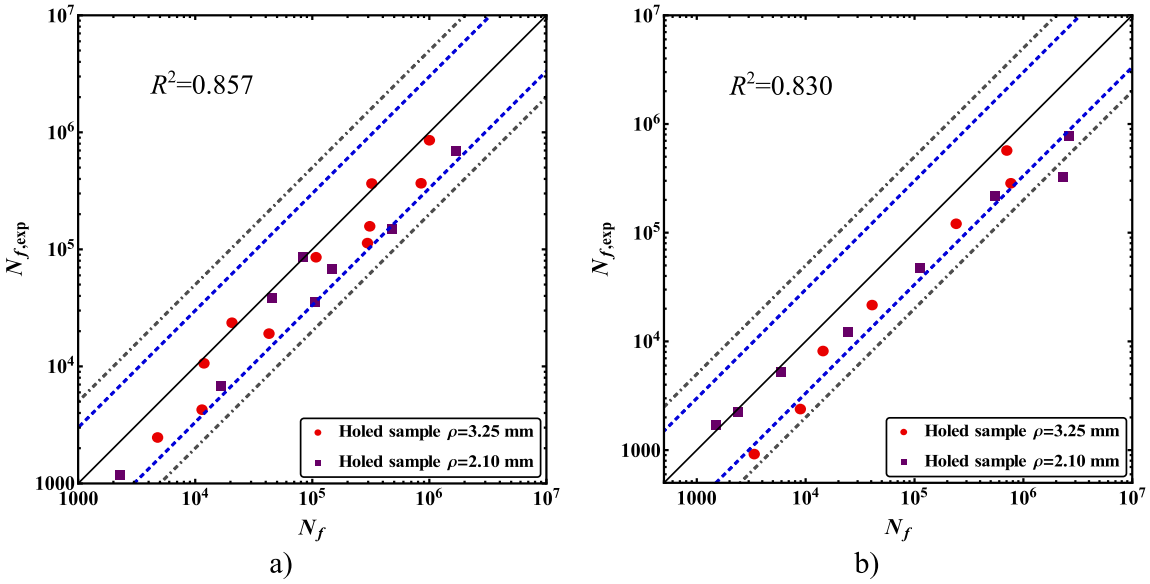

Fig. 11. Number of cycles to failure: experimental data $N_{f,exp}$ vs. TCD predictions N_f, for (a) $[90/0]_{2s}$ and (b) $[0/90]_{2s}$. The dashed blue lines represent the scatter bands of 1/3 and 3, whereas the dotted-dashed gray lines illustrate the scatter bands of 1/5 and 5.

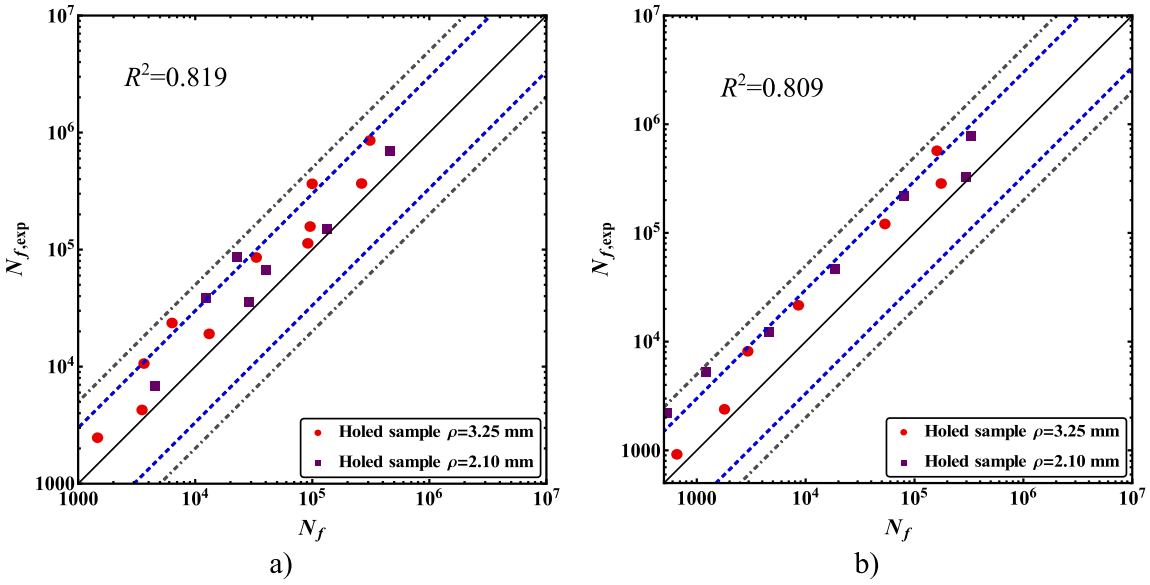

Fig. 12. Number of cycles to failure: experimental data, $N_{f,exp}$ vs. FFM predictions, N_f, for (a) $[90/0]_{2s}$, and (b) $[0/90]_{2s}$. The dashed blue lines represent the scatter bands of 1/3 and 3, whereas the dotted-dashed gray lines illustrate the scatter bands of 1/5 and 5.

normalized with respect to the strength of unnotched samples for 1000 cycles ($\sigma_{c,90/0}$ and $\sigma_{c,0/90}$ for each stacking sequence, respectively). Furthermore, the values for stress amplitude are chosen in such a way as to compare the size effect behavior of the two layups for a constant absolute value and a constant relative value with respect to their strength of unnotched samples for 1000 cycles. Note that N_f is expected to be greater than 1000 for sufficiently small holes, since the normalized applied stress is less than 1.

Fig. 13 provides several insights: (I) similarly to the static case, the results demonstrate that increasing the hole radius leads to a decrease in the amplitude of applied stress required to achieve the same fatigue life (Fig. 13a). On the other hand, for fixed applied stress, the fatigue life

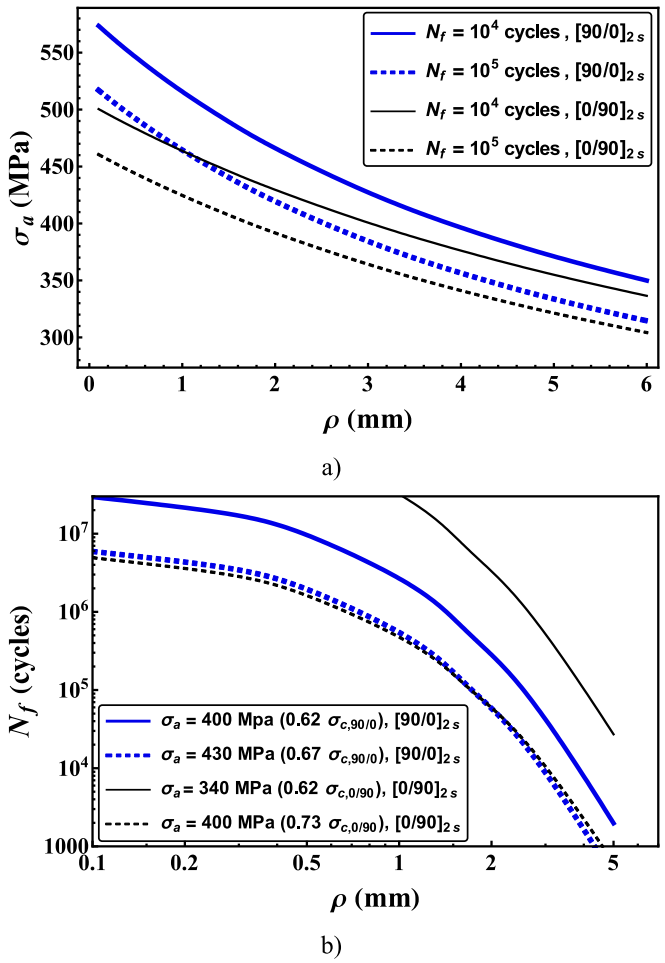

Fig. 13. Effect of the hole radius on nominal (gross-section) stress amplitude for constant fatigue lives (a), and on the fatigue life for fixed stress amplitudes in the log-log plane (b).

decreases with an increasing hole radius (Fig. 13b); (II) when considering fixed lifetimes, the performance of the layups exhibits a greater disparity for smaller hole sizes or, equivalently, both layups tend to exhibit similar performance as the notch radius increases; (III) the $[90/0]_{2s}$ layup exhibits better fatigue performance in terms of lifetime compared to the $[0/90]_{2s}$ layup, as seen in Fig. 7; (IV) based on Fig. 13a, it can be argued that $[90/0]_{2s}$ is slightly more sensitive to notches; this is evident from the higher slope of the representing curves.

6. Conclusions

TCD and FFM approaches were originally employed to assess the finite fatigue life of orthotropic drilled composites under tension-tension cyclic loading conditions. Moreover, the failure criteria can be employed in principle for any notch geometry or material, provided the failure mode is either a pullout or brittle failure. Both TCD and FFM models utilized two distinct input functions: the power-law relationships between the critical cyclic stress/the stress intensity factor and the number of cycles to failure. The former was obtained through stress-life data of plain specimens, whereas the latter was determined using stress-life data of cracked samples. To verify the proposed approach, a comprehensive experimental program was conducted covering a wide range of fatigue lives for two distinct layup configurations, $[0/90]_{2s}$ and $[90/0]_{2s}$, including plain, cracked, and two different notched specimens. The following conclusions can be drawn.

- The fatigue life estimation using both TCD and FFM models can be obtained rapidly without the need for sophisticated coding. Furthermore, in this study, the use of semi-analytical methods for calculating stress fields and stress intensity factors in orthotropic plates allowed us to obtain a straightforward solution.
- Without any inverse calibration of material properties and following standard testing procedures, it was demonstrated that both TCD and FFM models provide promising results in predicting the fatigue lives of composites, with a high degree of agreement between the models and experimental data.
- TCD was found to offer slightly higher accuracy, albeit slightly unconservative, while FFM results tended to be more conservative. On the other hand, for the $[0/90]_{2s}$ layup, the critical distance exceeded the ligament of the specimen with a smaller hole radius. This proves one notable advantage of FFM over TCD: the critical distance is not only a function of material properties, but also of the geometrical features.
- In general, the $[90/0]_{2s}$ layup exhibited superior fatigue strength when compared to the $[0/90]_{2s}$ layup. However, as the stress concentration increased from plain to crack, the difference in strength between the two layups decreased.
- For both layups, a behavior was observed in line with the conventional hole size effect, i.e., the number of cycles to failure for a given stress amplitude decreases as the hole radius increases.
- Parametric studies were conducted to investigate the impact of hole radius on the fatigue lifetime of both configurations. The results indicated that, as the hole size increases, the differences between the two layups decrease (as the stress concentration factor increases, see conclusion 4), whilst the $[90/0]_{2s}$ layup becomes more sensitive to the notch size.

Author statement

Amir Mohammad Mirzaei (corresponding author) conceived and designed the experiments, performed the data analysis, and wrote the manuscript (Conceptualization, Methodology, Formal analysis, Validation, Writing - Original Draft).

Amir Hossein Mirzaei conducted the experiments and wrote the manuscript (Investigation, Methodology, Validation, Writing - Original Draft).

Mahmood Mehrdad Shokrieh supervised the experiments, provided the facilities for testing, and reviewed the manuscript (Supervision, Resources, Writing - Review & Editing).

Alberto Sapora supervised the data analysis and reviewed the manuscript (Supervision, Validation, Writing - Review & Editing).

Pietro Cornetti supervised the data analysis and reviewed the manuscript (Supervision, Validation, Project administration, Writing - Review & Editing).

Declaration of competing interest

The authors declare that they have no known competing financial interests or personal relationships that could have appeared to influence the work reported in this paper.

Data availability

Data will be made available on request.

Acknowledgements

The authors Amir Mohammad Mirzaei, Alberto Sapora, and Pietro Cornetti would like to acknowledge the funding from the European Union's Horizon 2020 research and innovation program under the Marie Skłodowska-Curie grant agreement No 861061 – NEWFRAC Project.

References

[1] E.J. Barbero, Introduction to Composite Materials Design, CRC press, 2017.
[2] R.B. Pipes, R.C. Wetherhold, J.W. Gillespie Jr., Macroscopic fracture of fibrous composites, Mater. Sci. Eng. 45 (1980) 247–253, https://doi.org/10.1016/0025-5416(80)90153-6.
[3] P.K. Mallick, Fiber-reinforced Composites: Materials, Manufacturing, and Design, CRC press, 2007.
[4] S. Khandelwal, K.Y. Rhee, Recent advances in basalt-fiber-reinforced composites: tailoring the fiber-matrix interface, Composites, Part B 192 (2020), 108011, https://doi.org/10.1016/j.compositesb.2020.108011.
[5] S. Sihn, R.Y. Kim, K. Kawabe, S.W. Tsai, Experimental studies of thin-ply laminated composites, Compos. Sci. Technol. 67 (2007) 996–1008, https://doi.org/10.1016/j.compscitech.2006.06.008.
[6] Y. Qiao, A.A. Deleo, M. Salviato, A study on the multi-axial fatigue failure behavior of notched composite laminates, Compos. Part A Appl. Sci. Manuf. 127 (2019), 105640, https://doi.org/10.1016/j.compositesa.2019.105640.
[7] A.M. Mirzaei, M.R. Ayatollahi, B. Bahrami, F. Berto, A new unified asymptotic stress field solution for blunt and sharp notches subjected to mixed mode loading, Int. J. Mech. Sci. 193 (2021), 106176, https://doi.org/10.1016/j.ijmecsci.2020.106176.
[8] M.M. Mirsayar, A novel multiscale model for mixed-mode fatigue crack growth in laminated composites, Int. J. Mech. Sci. 255 (2023), 108470, https://doi.org/10.1016/j.ijmecsci.2023.108470.
[9] P. Shabani, F. Taheri-Behrooz, S. Maleki, M. Hasheminasab, Life prediction of a notched composite ring using progressive fatigue damage models, Composites, Part B 165 (2019) 754–763, https://doi.org/10.1016/j.compositesb.2019.02.031.
[10] A. Afaghi-Khatibi, L. Ye, Y.-W. Mai, An experimental study of the influence of fibre–matrix interface on fatigue tensile strength of notched composite laminates, Composites, Part B 32 (2001) 371–377, https://doi.org/10.1016/S1359-8368(01)00012-9.
[11] A.H. Mirzaei, M.M. Shokrieh, Evolution of the temperature rise and damage in laminated composites with stress concentration under fatigue loading, Composites, Part B 254 (2023) 110607, https://doi.org/10.1016/j.compositesb.2023.110607.
[12] A. Gaurav, K.K. Singh, Fatigue behavior of FRP composites and CNT-Embedded FRP composites: a review, Polym. Compos. 39 (2018) 1785–1808, https://doi.org/10.1002/pc.24177.
[13] D. Rajpal, F.M.A. Mitrotta, C.A. Socci, J. Sodja, C. Kassapoglou, R. De Breuker, Design and testing of aeroelastically tailored composite wing under fatigue and gust loading including effect of fatigue on aeroelastic performance, Compos. Struct. 275 (2021), 114373, https://doi.org/10.1016/j.compstruct.2021.114373.
[14] P. Alam, D. Mamalis, C. Robert, C. Floreani, C.M. Ó Brádaigh, The fatigue of carbon fibre reinforced plastics - a review, Composites, Part B 166 (2019) 555–579, https://doi.org/10.1016/j.compositesb.2019.02.016.
[15] M.M. Shokrieh, L.B. Lessard, Progressive fatigue damage modeling of composite materials, Part I: modeling, J. Compos. Mater. 34 (2000) 1056–1080, https://doi.org/10.1177/002199830003401301.
[16] S. Mandegarian, F. Taheri-Behrooz, A general energy based fatigue failure criterion for the carbon epoxy composites, Compos. Struct. 235 (2020), 111804, https://doi.org/10.1016/j.compstruct.2019.111804.
[17] J.M. Whitney, R.J. Nuismer, Stress fracture criteria for laminated composites containing stress concentrations, J. Compos. Mater. 8 (1974) 253–265, doi: 10.1177/002199837400800303.
[18] G. Caprino, J.C. Halpin, L. Nicolais, Fracture mechanics in composite materials, Composites 10 (1979) 223–227, doi: 10.1016/0010-4361(79)90023-5.
[19] P.P. Camanho, P. Maimí, C.G. Dávila, Prediction of size effects in notched laminates using continuum damage mechanics, Compos. Sci. Technol. 67 (2007) 2715–2727, https://doi.org/10.1016/j.compscitech.2007.02.005.
[20] R.B. Pipes, R.C. Wetherhold, J.W. Gillespie Jr., Notched strength of composite materials, J. Compos. Mater. 13 (1979) 148–160, doi: 10.1177/002199837901300206.
[21] R.B. Pipes, J.W. Gillespie Jr., R.C. Wetherhold, Superposition of the notched strength of composite laminates, Polym. Eng. Sci. 19 (1979) 1151–1155, doi: 10.1002/pen.760191604.
[22] H.M.S. Belmonte, C.I.C. Manger, S.L. Ogin, P.A. Smith, R. Lewin, Characterisation and modelling of the notched tensile fracture of woven quasi-isotropic GFRP laminates, Compos. Sci. Technol. 61 (2001) 585–597, https://doi.org/10.1016/S0266-3538(00)00238-4.
[23] O.A. Khondker, I. Herszberg, H. Hamada, Measurements and prediction of the compression-after-impact strength of glass knitted textile composites, Compos. Part A Appl. Sci. Manuf. 35 (2004) 145–157, https://doi.org/10.1016/j.compositesa.2003.10.008.
[24] J.S. Huh, W. Hwang, Fatigue life prediction of circular notched CFRP laminates, Compos. Struct. 44 (1999) 163–168, https://doi.org/10.1016/S0263-8223(98)00128-7.
[25] D. Taylor, Geometrical effects in fatigue: a unifying theoretical model, Int. J. Fatig. 21 (1999) 413–420, https://doi.org/10.1016/S0142-1123(99)00007-9.
[26] D. Taylor, The Theory of Critical Distances: A New Perspective in Fracture Mechanics, Elsevier, Oxford, 2007, https://doi.org/10.1016/B978-0-08-044478-9.X5000-5.
[27] D. Morgan, S. Quinlan, D. Taylor, Using the theory of critical distances to predict notch effects in fibre composites, Theor. Appl. Fract. Mech. 118 (2022) 103285, https://doi.org/10.1016/j.tafmec.2022.103285.
[28] F.T. Ibáñez-Gutiérrez, S. Cicero, Fracture assessment of notched short glass fibre reinforced polyamide 6: an approach from failure assessment diagrams and the theory of critical distances, Composites, Part B 111 (2017) 124–133, doi: 10.1016/j.compositesb.2016.11.053.
[29] F.T. Ibáñez-Gutiérrez, S. Cicero, I.A. Carrascal, I. Procopio, Effect of fibre content and notch radius in the fracture behaviour of short glass fibre reinforced polyamide 6: an approach from the Theory of Critical Distances, Composites, Part B 94 (2016) 299–311, https://doi.org/10.1016/j.compositesb.2016.03.064.
[30] M.E. Waddoups, J.R. Eisenmann, B.E. Kaminski, Macroscopic fracture mechanics of advanced composite materials, J. Compos. Mater. 5 (1971) 446–454, doi: 10.1177/002199837100500402.
[31] T.A. Cruse, Tensile strength of notched composites, J. Compos. Mater. 7 (1973) 218–229, doi: 10.1177/002199837300700206.
[32] R. Prabhakaran, Tensile fracture of composites with circular holes, Mater. Sci. Eng. 41 (1979) 121–125, https://doi.org/10.1016/0025-5416(79)90051-X.
[33] M.-L. Antti, E. Lara-Curzio, R. Warren, Thermal degradation of an oxide fibre (Nextel 720)/aluminosilicate composite, J. Eur. Ceram. Soc. 24 (2004) 565–578, https://doi.org/10.1016/S0955-2219(03)00250-4.
[34] P.K. Govindan Potti, B.N. Rao, V.K. Srivastava, Notched tensile strength for long- and short-fiber reinforced polyamide, Theor. Appl. Fract. Mech. 33 (2000) 145–152, https://doi.org/10.1016/S0167-8442(00)00009-4.
[35] D. Leguillon, Strength or toughness? A criterion for crack onset at a notch, Eur. J. Mech. 21 (2002) 61–72, https://doi.org/10.1016/S0997-7538(01)01184-6.
[36] P. Cornetti, N. Pugno, A. Carpinteri, D. Taylor, Finite fracture mechanics: a coupled stress and energy failure criterion, Eng. Fract. Mech. 73 (2006) 2021–2033, https://doi.org/10.1016/j.engfracmech.2006.03.010.
[37] A.M. Mirzaei, M. Corrado, A. Sapora, P. Cornetti, Analytical modeling of debonding mechanism for long and short bond lengths in direct shear tests accounting for residual strength, Materials 14 (2021), https://doi.org/10.3390/ma14216690.
[38] R. Dimitri, P. Cornetti, V. Mantič, M. Trullo, L. De Lorenzis, Mode-I debonding of a double cantilever beam: a comparison between cohesive crack modeling and Finite Fracture Mechanics, Int. J. Solid Struct. 124 (2017) 57–72, https://doi.org/10.1016/j.ijsolstr.2017.06.007.
[39] P.P. Camanho, G.H. Erçin, G. Catalanotti, S. Mahdi, P. Linde, A finite fracture mechanics model for the prediction of the open-hole strength of composite laminates, Compos. Part A Appl. Sci. Manuf. 43 (2012) 1219–1225, https://doi.org/10.1016/j.compositesa.2012.03.004.
[40] G. Catalanotti, P.P. Camanho, A semi-analytical method to predict net-tension failure of mechanically fastened joints in composite laminates, Compos. Sci. Technol. 76 (2013) 69–76, doi: 10.1016/j.compscitech.2012.12.009.
[41] X. Li, Z. Xie, W. Zhao, Y. Zhang, Y. Gong, N. Hu, Failure prediction of irregular arranged multi-bolt composite repair based on finite fracture mechanics model, Eng. Fract. Mech. 242 (2021) 107456, https://doi.org/10.1016/j.engfracmech.2020.107456.
[42] J. Felger, N. Stein, W. Becker, Mixed-mode fracture in open-hole composite plates of finite-width: an asymptotic coupled stress and energy approach, Int. J. Solid Struct. 122 (2017) 14–24, doi: 10.1016/j.ijsolstr.2017.05.039.
[43] C. Furtado, A. Arteiro, M.A. Bessa, B.L. Wardle, P.P. Camanho, Prediction of size effects in open-hole laminates using only the Young's modulus, the strength, and the R-curve of the 0° ply, Compos. Part A Appl. Sci. Manuf. 101 (2017) 306–317, https://doi.org/10.1016/j.compositesa.2017.04.014.
[44] J. Reinoso, A. Arteiro, M. Paggi, P.P. Camanho, Strength prediction of notched thin ply laminates using finite fracture mechanics and the phase field approach, Compos. Sci. Technol. 150 (2017) 205–216, doi: 10.1016/j.compscitech.2017.07.020.
[45] A.M. Mirzaei, P. Cornetti, A. Sapora, A novel Finite Fracture Mechanics approach to assess the lifetime of notched components, Int. J. Fatig. (2023), 107659, https://doi.org/10.1016/j.ijfatigue.2023.107659.
[46] A. Sapora, P. Cornetti, A. Campagnolo, G. Meneghetti, Fatigue limit: crack and notch sensitivity by finite fracture mechanics, Theor. Appl. Fract. Mech. 105 (2020), 102407, https://doi.org/10.1016/j.tafmec.2019.102407.
[47] J. Galos, Thin-ply composite laminates: a review, Compos. Struct. 236 (2020), 111920, https://doi.org/10.1016/j.compstruct.2020.111920.
[48] H.J. Konish, J.M. Whitney, Approximate stresses in an orthotropic plate containing a circular hole, J. Compos. Mater. 9 (1975) 157–166, https://doi.org/10.1177/002199837500900206.
[49] A. Sapora, A.R. Torabi, S. Etesam, P. Cornetti, Finite Fracture Mechanics crack initiation from a circular hole, Fatig. Fract. Eng. Mater. Struct. 41 (2018) 1627–1636, https://doi.org/10.1111/ffe.12801.
[50] G. Catalanotti, R.M. Salgado, P.P. Camanho, On the Stress Intensity Factor of cracks emanating from circular and elliptical holes in orthotropic plates, Eng. Fract. Mech. 252 (2021), 107805, https://doi.org/10.1016/j.engfracmech.2021.107805.
[51] J.C. Newman Jr., A Nonlinear Fracture Mechanics Approach to the Growth of Small Cracks, 1983.
[52] H. Tada, P.C. Paris, G.R. Irwin, The Stress Analysis of Cracks, vol. 34, Del Res. Corp., Handbook, 1973.
[53] G. Bao, S. Ho, Z. Suo, B. Fan, The role of material orthotropy in fracture specimens for composites, Int. J. Solid Struct. 29 (1992) 1105–1116, https://doi.org/10.1016/0020-7683(92)90138-J.
[54] Z. Suo, G. Bao, B. Fan, T.C. Wang, Orthotropy rescaling and implications for fracture in composites, Int. J. Solid Struct. 28 (1991) 235–248, https://doi.org/10.1016/0020-7683(91)90208-W.
[55] L. Susmel, D. Taylor, A novel formulation of the theory of critical distances to estimate lifetime of notched components in the medium-cycle fatigue regime, Fatig. Fract. Eng. Mater. Struct. 30 (2007) 567–581, doi: 10.1111/j.1460-2695.2007.01122.x.

[56] O.H. Basquin, The Exponential Law of Endurance Tests, Proc Am Soc Test Mater, 1910, pp. 625–630.
[57] M. Ciavarella, P. D'Antuono, G.P. Demelio, Generalized definition of "crack-like" notches to finite life and SN curve transition from "crack-like" to "blunt notch" behavior, Eng. Fract. Mech. 179 (2017) 154–164, https://doi.org/10.1016/j.engfracmech.2017.04.048.
[58] A. Carpinteri, M. Paggi, A unified interpretation of the power laws in fatigue and the analytical correlations between cyclic properties of engineering materials, Int. J. Fatig. 31 (2009) 1524–1531, https://doi.org/10.1016/j.ijfatigue.2009.04.014.
[59] P.P. Camanho, G. Catalanotti, On the relation between the mode I fracture toughness of a composite laminate and that of a 0° ply: analytical model and experimental validation, Eng. Fract. Mech. 78 (2011) 2535–2546, https://doi.org/10.1016/j.engfracmech.2011.06.013.
[60] A.H. Mirzaei, M.M. Shokrieh, A. Saeedi, Fatigue behavior of laminated composites with embedded SMA wires, Compos. Struct. (2022) 115753, https://doi.org/10.1016/j.compstruct.2022.115753.
[61] A.H. Mirzaei, M.M. Shokrieh, Simulation and measurement of the self-heating phenomenon of carbon/epoxy laminated composites under fatigue loading, Composites, Part B 223 (2021) 109097, https://doi.org/10.1016/j.compositesb.2021.109097.
[62] W. Roundi, A. El Mahi, A. El Gharad, J.-L. Rebière, Experimental and numerical investigation of the effects of stacking sequence and stress ratio on fatigue damage of glass/epoxy composites, Composites, Part B 109 (2017) 64–71, doi: 10.1016/j.compositesb.2016.10.044.
[63] B.G. Green, M.R. Wisnom, S.R. Hallett, An experimental investigation into the tensile strength scaling of notched composites, Compos. Part A Appl. Sci. Manuf. 38 (2007) 867–878, doi: 10.1016/j.compositesa.2006.07.008.
[64] C.E. Harris, D.H. Morris, Role of Delamination and Damage Development on the Strength of Thick Notched Laminates, ASTM International, 1985.
[65] R.S. Vaidya, J.C. Klug, C.T. Sun, Effect of ply thickness on fracture of notched composite laminates, AIAA J. 36 (1998) 81–88.
[66] Standard test method for tensile properties of polymer matrix composite materials, ASTM D3039/DM. 3039, https://doi.org/10.1520/D3039_D3039M-17, 2008.
[67] Standard test method for in-plane shear response of polymer matrix composite materials by tensile test of a ±45° laminate, ASTM D3171-22, https://doi.org/10.1520/D3518_D3518M-18, 2018.
[68] Standard test methods for constituent content of composite materials, ASTM D3171-22, https://doi.org/10.1520/D3171-22, 2022.